

1 **Lineage tracing of *Shh*⁺ floor plate cells and dynamics of dorsal-ventral**
2 **gene expression in the regenerating axolotl spinal cord**

3 **Laura I. Arbanas^{1,2}, Emanuel Cura Costa³, Osvaldo Chara^{4,5,6}, Leo Otsuki^{1,2,#}, Elly**
4 **M. Tanaka^{1,2,#}**

5 ¹ Institute of Molecular Biotechnology of the Austrian Academy of Sciences (IMBA), Vienna
6 BioCenter (VBC), Dr. Bohr-Gasse 3, 1030 Vienna, Austria

7 ² Research Institute of Molecular Pathology (IMP), Vienna BioCenter (VBC), Campus-
8 Vienna-Biocenter 1, 1030 Vienna, Austria

9 ³ Institute of Physics of Liquids and Biological Systems (IFLYSIB), National Scientific and
10 Technical Research Council (CONICET), University of La Plata, La Plata B1900BTE,
11 Argentina

12 ⁴ School of Biosciences, University of Nottingham, Sutton Bonington Campus, Nottingham
13 LE12 5RD, United Kingdom

14 ⁵ Center for Information Services and High Performance Computing, Technische Universität
15 Dresden, Dresden, Germany

16 ⁶ Instituto de Tecnología, Universidad Argentina de la Empresa, Buenos Aires, Argentina

17 [#] Corresponding authors: Leo Otsuki (leo.otsuki@imba.oeaw.ac.at) and Elly M Tanaka
18 (elly.tanaka@imba.oeaw.ac.at).

19 **Abstract**

20 Both development and regeneration depend on signalling centres, which are sources of
21 locally secreted tissue-patterning molecules. As many signalling centres are decommissioned
22 before the end of embryogenesis, a fundamental question is how signalling centres can be re-
23 induced later in life to promote regeneration after injury. Here, we use the axolotl salamander
24 model (*Ambystoma mexicanum*) to address how the floor plate is assembled for spinal cord
25 regeneration. The floor plate is an archetypal vertebrate signalling centre that secretes *Shh*
26 ligand and patterns neural progenitor cells during embryogenesis. Unlike mammals, axolotls
27 continue to express floor plate genes (including *Shh*) and downstream dorsal-ventral
28 patterning genes in their spinal cord throughout life, including at steady state. The
29 parsimonious hypothesis that *Shh*⁺ cells give rise to functional floor plate cells for
30 regeneration had not been tested. Using HCR *in situ* hybridisation and mathematical
31 modelling, we first quantitated the behaviours of dorsal-ventral spinal cord domains,
32 identifying significant increases in gene expression level and floor plate size during
33 regeneration. Next, we established a transgenic axolotl to specifically label and fate map
34 *Shh*⁺ cells *in vivo*. We found that labelled *Shh*⁺ cells gave rise to regeneration floor plate,
35 and not to other neural progenitor domains, after tail amputation. Thus, despite changes in
36 domain size and downstream patterning gene expression, *Shh*⁺ cells retain their floor plate
37 identity during regeneration, acting as a stable cellular source for this regeneration signalling
38 centre in the axolotl spinal cord.

39 **Key words**

40 Spinal cord, Regeneration, Stem cells, Floor plate, Axolotl

41 **Introduction**

42 Understanding how to regenerate the spinal cord after injury is a central question in
43 regenerative research. Regenerative species such as axolotls (*Ambystoma mexicanum*) and
44 zebrafish (*Danio rerio*) have revealed that important contributors to spinal cord regeneration
45 are resident neural progenitor cells (also known as neural stem cells, ependymal glial cells or
46 ependymoglia radial cells). These progenitors, which line the central canal of the spinal cord,
47 can replace tissue lost or damaged in several injury paradigms in salamanders and zebrafish,
48 such as crush injury (Hui et al., 2010; Thygesen et al., 2019; Walker et al., 2023), transection
49 injury (Becker et al., 1997; Piatt, 1955) or a full tail amputation (Egar and Singer, 1972). For
50 example, amputation of the axolotl spinal cord recruits neural progenitors residing within a
51 ~800 μ m zone to switch to fast, proliferative cell divisions (Albors et al., 2015; Cura Costa
52 et al., 2021; Mchedlishvili et al., 2007; Rost et al., 2016), generating a neuroepithelial tube
53 that differentiates into a functional spinal cord.

54 The embryonic origin of spinal cord neural progenitors, and their patterning, is well
55 understood in mouse (*Mus musculus*) and chicken (*Gallus gallus*). In these species, two major
56 signalling centres in the developing neural plate generate opposing morphogen gradients that
57 provide dorsal-ventral positional information (reviewed in (Sagner and Briscoe, 2019)). The
58 dorsally located roof plate secretes Bone Morphogenetic Protein (BMP) family members
59 (Liem et al., 1997) and *Wnt*-family proteins (Muroyama et al., 2002), while the ventrally
60 located floor plate secretes Sonic hedgehog (*Shh*) (Echelard et al., 1993). Neural progenitors
61 residing between the two signalling centres receive different concentrations and durations of
62 signalling molecules and acquire distinct dorsal-ventral identities. As a result, neural

63 progenitors express different transcription factors depending on their location (e.g. *Pax7* and
64 *Msx1* dorsally, *Pax6* laterally, *Nkx6.1* ventro-laterally) and generate distinct neuron subtypes
65 (reviewed by (Sagner and Briscoe, 2019)). Towards the end of embryogenesis, the mouse
66 spinal cord undergoes molecular changes: *Shh* signalling is extinguished (Cañizares et al.,
67 2020), BMP activity extends ventrally (Cañizares et al., 2020) and the expression of dorsal-
68 ventral patterning genes is altered or diminished (Albors et al., 2023; Ghazale et al., 2019).
69 The adult mouse spinal cord regenerates poorly and resident ependymal cells generate a glial
70 scar after injury (Meletis et al., 2008) instead of restoring neurons and function.

71 An interesting possibility is that instilling an embryo-like arrangement of roof plate,
72 lateral progenitors and floor plate during adulthood would contribute to reconstitution of
73 developmental mechanisms and replace lost neurons. Regenerative axolotls indeed express
74 roof plate genes (*Msx1*, *Pax7*, *BMP2*), lateral patterning genes (*Pax6*) and floor plate genes
75 (*Shh*, *FoxA2*) in this manner throughout life (Schnapp et al., 2005; Sun et al., 2018). It is
76 tempting to speculate that this arrangement acts as a template to launch appropriate gene
77 cascades and replace missing spinal cord regions after injury. In adult zebrafish, the
78 expression of *shha*, *nkx6.1*, *pax6* and *olig2* increases locally following spinal cord transection
79 (Reimer et al., 2009), which could reflect the activation of such gene cascades. In axolotls,
80 *Pax6* and *Pax7* expression decrease 1 day post-tail amputation (Albors et al., 2015), but the
81 later expression dynamics of these, and other, genes have not been quantified. Elucidating
82 the dynamics of dorsal-ventral gene expression after axolotl tail amputation could illuminate
83 mechanisms of spinal cord regeneration conserved across injury paradigms and species.

84 Here, we quantified the expression of dorsal-ventral patterning genes covering roof
85 plate to floor plate during axolotl spinal cord regeneration. Using mathematical modelling,

86 we extracted gene expression levels and the relative sizes of the dorsal-ventral domains from
87 measurements made with single molecule fluorescent *in situ* hybridisation (smFISH). We
88 found that dorsal-ventral genes increased their expression after amputation, similar to
89 zebrafish transection, but additionally discovered changes in the representation of the dorsal-
90 ventral domains. In particular, we found that the *Shh*⁺ floor plate almost doubles in size,
91 which is relevant considering that it is an essential signalling centre for regeneration:
92 pharmacological inhibition of *Shh* signalling results in an expanded dorsal domain and blocks
93 axolotl spinal cord outgrowth (Schnapp et al., 2005).

94 The expansion of the *Shh*⁺ domain prompted us to address how *Shh*⁺ floor plate cells
95 contribute to the regenerated spinal cord. If continuous *Shh*⁺ expression reflects a cellular
96 memory and fate restriction, floor plate cells would be expected to produce only floor plate
97 cells during regeneration. However, lineage tracing of single electroporated cells have
98 suggested that axolotl progenitors can change dorsal-ventral identity (Mchedlishvili et al.,
99 2007). Given the expression of ventrally-derived *Shh*, it is plausible that neighbouring
100 progenitors could change between medio-lateral, lateral and dorsal fates but whether *Shh*⁺
101 floor plate cells themselves remain lineage-restricted, or can change identities, was not
102 determined (Mchedlishvili et al., 2007). We performed genetic fate mapping of *Shh*⁺ floor
103 plate cells and found that they exclusively generate more floor plate during axolotl spinal
104 cord regeneration, supporting a fate restriction model.

105 **Materials and methods**

106 **Axolotl (*Ambystoma mexicanum*) husbandry**

107 All procedures were approved by the Magistrate of Vienna Genetically Modified Organism
108 Office and MA58, City of Vienna, Austria (licences: GZ:51072/2019/16, GZ: MA58-
109 1432587-2022-12, GZ: MA58-1516101-2023-21). Axolotls were raised in Vienna tap water.
110 Axolotl breedings were performed at the IMP by the animal caretaker team. Axolotl sizes are
111 reported in cm, measured from snout to tail tip. Axolotl surgeries, live imaging and tissue
112 harvesting were performed under anaesthesia in 0.015% benzocaine (Sigma-Aldrich E1501,
113 preparation according to (Khattak et al., 2014)). Tail amputations were performed between
114 myotome 8-10 post-cloaca (3-4 cm animals) or halfway between cloaca and tail tip (1.5-2
115 cm animals (lineage tracings)).

116

117 **Axolotl genome and transcriptome reference**

118 Axolotl genome assembly AmexG_v6.0-DD and transcriptome assembly AmexT_v47
119 (Schloissnig et al., 2021).

120

121 **Generation of *Shh* knock-in axolotl**

122 *Shh* knock-in axolotl “*Shh*^{EGFP-dERC}” (tm(*Shh*^{t/+}:*Shh*-P2A-myr-EGFP-T2A-*ER*^{T2}-*Cre*-
123 *ER*^{T2})^{Etnka}) was generated by CRISPR/Cas9 and NHEJ-mediated knock-in into the last intron
124 of the *Shh* gene (Fei et al., 2018). De-jellied, 1-cell stage axolotl eggs were injected with

125 injection mix as described in (Khattak et al., 2014), delivered as 2 x 2.5 nl shots. Injection
126 mix recipe: 5 µg Cas9-NLS protein, 4 µg *Shh* gRNA, 0.5 µg *Shh* knock-in cassette, 1 µl Cas9
127 buffer, diluted to 10 µl in water. Cas9-NLS protein and Cas9 buffer were prepared by the
128 Vienna Biocenter Core Facilities. Axolotls with successful knock-in were recovered by
129 screening for EGFP fluorescence in the posterior limb bud at embryo stage 42-44 using an
130 AXIOzoom V16 microscope (Zeiss). Transgenic individuals were reared to sexual maturity
131 and germline-transmitted offspring were used in all experiments.

132 *Shh* gRNA was prepared as described in (Fei et al., 2018) by PCR amplification and
133 *in vitro* transcription of the following synthesised oligonucleotides (purchased from Merck):

134 >*Shh*-gRNA oligo_FWD (target sequence in *Shh* last intron is underlined)

135 GAAATTAATACGACTCACTATAGGGCGTACTTCTGGACTTGGGTTTAGAGCTA

136 GAAATAGC

137 >Common-gRNA-REV (Fei et al., 2018)

138 AAAAGCACCGACTCGGTGCCACTTTCAAGTTGATAACGGACTAGCCTTATT

139 TAACTTGCTATTCTAGCTCTA AAAC

140 *Shh* knock-in cassette was assembled in a plasmid by Gibson Assembly, purified
141 using a Plasmid Maxi Kit (Qiagen 12163) and verified by Sanger sequencing prior to egg
142 injection. Knock-in cassette encodes: last *Shh* intron and exon, P2A ‘self-cleaving’ sequence,
143 EGFP fluorescent protein fused with a N-myristoylation sequence, T2A ‘self-cleaving’
144 sequence, tamoxifen-inducible Cre recombinase, poly-adenylation sequence.

145

146 **Other axolotl strains**

147 The following published axolotl strains were used in this study: *d/d* (control strain),
148 *tm(Pax7^{+/+}:Pax7-P2A-memCherry-T2A-ER^{T2}-Cre-ER^{T2})^{Etnka}* (Fei et al., 2017),
149 *tgSceI(Caggs:loxP-GFP-dead(Stop)-loxP-mCherry)^{Etnka}* (Kawaguchi et al., 2024),
150 *tgSceI(Caggs:loxP-GFP-loxP-mCherry)^{Etnka}* (Khattak et al., 2013). Nomenclature is
151 according to (Nowoshilow et al., 2021).

152

153 **Genetic lineage tracing of *Shh*⁺ cells**

154 *Shh^{EGFP-dERC}* axolotls were mated with memory cassette axolotls of genotype
155 *tgSceI(Caggs:loxP-GFP-dead(Stop)-loxP-mCherry)^{Etnka}* (Kawaguchi et al., 2024).
156 (Kawaguchi et al., 2024) To induce Cre/loxP-mediated recombination, progeny axolotls were
157 treated with 4-hydroxytamoxifen (4-OHT) by bathing, as described in the water-based
158 method of (Khattak et al., 2014). 3 cm axolotls were amputated halfway between cloaca and
159 tail tip and bathed overnight in the dark on days 1, 3 and 5 post-amputation with 2 µM 4-
160 OHT. Successfully recombined individuals were identified by screening for mCherry
161 expression 7 days after the last 4-OHT treatment using an AXIOZoom V16 microscope
162 (Zeiss). For lineage tracing, tails were re-amputated <500 µm posterior to mCherry⁺ cells.
163 Tail offcuts containing mCherry⁺ cells were harvested to test the fidelity of labelling.
164 Animals were left to regenerate for 7 days (“short-term tracing”) or 28 days (“long-term
165 tracing”) before harvesting.

166

167 **Live imaging**

168 Axolotls were anaesthetised in 0.015% benzocaine (Sigma-Aldrich E1501, preparation
169 according to (Khattak et al., 2014)) and imaged using an AXIOzoom V16 microscope (Zeiss)
170 on the indicated days post-tail amputation. Axolotls were returned to tap water immediately
171 after imaging.

172

173 **Tissue harvesting and cryosectioning**

174 Axolotl tails were harvested and fixed overnight at 6°C in 4% paraformaldehyde (PFA), pH
175 7.4. Fixed samples were washed twice with cold PBS then incubated sequentially with the
176 following solutions overnight at 6°C: (1) 20% sucrose in PBS, (2) 30% sucrose in PBS, then
177 incubated for 3 hours in a 1:1 mix of 30% sucrose/PBS and Tissue-Tek O.C.T. compound
178 (Sakura). Samples were embedded in O.C.T., frozen on dry ice and sectioned immediately
179 (20 µm thickness) or stored at -70 °C. Slides were stored at -20 °C until use.

180

181 **Immunofluorescent staining of tissue sections**

182 Slides were brought to room temperature and washed with PBS to remove O.C.T. For DAPI
183 staining only: slides were incubated with 10 µg/ml DAPI solution (Sigma-Aldrich D9542)
184 for 30 mins at room temperature, then washed well with PBS. For immunostaining against
185 PAX6, PAX7 and SOX2: slides were incubated for 1 hour at room temperature in blocking

186 solution (PBS containing 1% BSA (bovine serum albumin) and 0.5% Triton X-100). Slides
187 were incubated overnight at 6°C with primary antibodies diluted in blocking solution. The
188 following day, all slides were washed three times over 3 hours at room temperature with
189 blocking solution. Slides were incubated overnight at 6°C with secondary antibodies diluted
190 in blocking solution. Finally, slides were washed three times with blocking solution and once
191 in PBS before mounting in Abberior MOUNT embedding media for imaging. For
192 immunostaining against SHH: antigen retrieval was necessary. After washing off O.C.T.,
193 slides were incubated in undiluted 10X citrate buffer (Dako) for 45 minutes at 65 °C, then
194 washed twice in PBS before blocking and proceeding to antibody staining as for the other
195 antigens. Images were acquired using a spinning disk confocal setup (Olympus IX83 inverted
196 microscope / Yokogawa CSU-W1) and a 40x air objective. Primary antibodies and dilutions
197 used were: anti-PAX6 (rabbit, Biolegend, #901301, 1:200), anti-PAX7 (mouse, DSHB,
198 #Pax7-s, 1:100), anti-SHH (rabbit, Cell Signalling Technologies, #2207S, 1:200), anti-SOX2
199 (rat, eBioscience, Btjce, 1:200). Primary antibodies were detected using secondary antibodies
200 conjugated to Alexa fluorophores (Thermo Fisher Scientific).

201

202 **HCR staining of tissue sections and HCR probe design**

203 Slides were brought to room temperature and washed with PBS to remove O.C.T. HCR *in*
204 *situ* hybridisation was performed according to the HCR RNA-FISH protocol for fresh/fixed
205 frozen tissue sections (Molecular Instruments, (Choi et al., 2018)), omitting the post-fixation
206 and proteinase K treatment steps. Probe hybridisation buffer, wash buffer, amplification
207 buffer and detection hairpins were purchased from Molecular Instruments. Probe

208 hybridisation was performed at 37 °C for 18 h. Amplification was performed at room
209 temperature for 18-20 h using B1/B2/B5 hairpins conjugated to Alexa-546 or Alexa-647
210 fluorophores. Following the HCR procedure, slides were incubated with 10 µg/ml DAPI
211 solution (Sigma-Aldrich D9542) for 30 mins at room temperature, then washed well with
212 PBS. Samples were mounted in Abberior MOUNT embedding media for imaging. Images
213 were acquired using a spinning disk confocal setup (Olympus IX83 inverted microscope /
214 Yokogawa CSU-W1) and a 40x air objective.

215 HCR probes were designed against unique mRNA sequences identified by BLAST
216 alignment against axolotl transcriptome Amex.T_v47 (Schloissnig et al., 2021). Sequences
217 were considered unique if they did not match off-target sequences at more than 36 out of 50
218 consecutive nucleotides. HCR probes targeting axolotl *Shh* mRNA (Otsuki et al., 2023) were
219 purchased from Molecular Instruments; all other probes (*Nkx6.1*, *Pax6*, *Pax7*, *Msx1*, *Sox2*)
220 were purchased as oPools at 50 pmol scale from IDT (Integrated DNA Technologies).

221

222 **Fluorescence intensity quantifications**

223 Image quantifications were performed using Fiji software (Schindelin et al., 2012). The
224 segmented line tool was used to draw a line trajectory through the region of interest (line
225 thickness: “100” for HCR experiments (measurements were made on maximum intensity
226 projections of 20 µm) and “10” for live dual reporter experiments. The Measure function was
227 used to extract continuous mean gray values for analysis.

228

229 **Mathematical modelling of fluorescence data**

230 A detailed description of the mathematical modelling can be found in the Supplementary
231 Information. We used a piecewise constant model in which spatial domains of constant signal
232 are separated by one or more switch points (see Figure S1a). We used a two-step model
233 variant for *Msx1*, *Pax7*, *Nkx6.1* and *Shh* (two domains separated by one switch point), and a
234 three-step model variant for *Pax6* (three domains separated by two switch points). We
235 determined domain size by fitting the relevant model to the HCR signal data and inferring
236 the switch point(s). To estimate gene expression, we calculated average HCR signal
237 intensities on either side of the switch point(s) and subtracted background signal from
238 expression signal.

239 To determine the optimal fits, the mean signal levels for the zones defined by the
240 switch point in the two-step function (or pairs of switch points in the three-step function)
241 were determined. Next, the switch points were systematically varied across the data range.
242 For each potential switch point, the mean signal levels in the resulting zones were calculated.
243 To assess the best-fitting parameter values, the sum of squared errors (SSE) was calculated.
244 See Supplementary Information for details on SSE and all individual fits to the HCR data.

245

246 **Statistics and data representation**

247 Statistical analysis and graph plotting were performed using custom Python scripts
248 (mathematical analyses) or in Prism software (GraphPad; all other analyses). The Python
249 scripts utilised several Python libraries: SciPy for statistical analysis (Virtanen et al., 2020),

250 NumPy for numerical computations (Harris et al., 2020) and Matplotlib (Hunter, 2007) and
251 Seaborn (Waskom, 2021) for visualisation. Statistical tests are defined in the figure legends
252 and statistical significance was considered as $p < 0.05$. Figures were assembled in Adobe
253 Illustrator.

254

255 **Code availability**

256 The code used in this study is available on Github (<https://github.com/ecuracosta/dorsal->
257 ventral_gene_expression_in_the_regeneration_axolotl_spinal_cord) and Zenodo (Cura
258 Costa and Chara, 2024).

259

260 **Results and discussion**

261 **Mathematical modelling of dorsal-ventral domains during spinal cord regeneration.**

262 First, we confirmed the protein expression domains of SOX2 (expressed in neural progenitor
263 cells) and the dorsal-ventral genes PAX7, PAX6 and SHH in steady state axolotl spinal cords
264 (Figure 1a). Next, to profile the expression of these genes during spinal cord regeneration,
265 we performed Hybridisation Chain Reaction (HCR) smFISH on tail sections harvested at
266 steady state or at 14 days post-tail amputation (14 dpa) (Figures 1b-c). We included the roof
267 plate gene *Msx1* in these assays as well as *Nkx6.1*, which had not been assayed previously in
268 axolotls. We found *Nkx6.1* to be expressed in floor plate and ventro-lateral progenitors in a
269 similar manner to the neural tube of mouse and chick (Figure 1c) (Briscoe et al., 2000; Qiu
270 et al., 1998; Sander et al., 2000). Between these genes, we could identify at least 4 molecular
271 domains whose arrangement appeared superficially similar between steady state and
272 regeneration (from dorsal to ventral: *Msx1*+*Pax7*+, *Pax7*+*Pax6*+, *Pax6*+*Nkx6.1*+,
273 *Nkx6.1*+*Shh*+) (Figure 1c).

274 How the expression levels and domain sizes of the dorsal-ventral genes change during
275 axolotl spinal cord regeneration is not known. To gain insights into these processes, we
276 measured HCR signal along a continuous dorsal-to-ventral line drawn through progenitors
277 contacting the spinal cord lumen (Figure 1d) (number of quantified sections is indicated in
278 Table 1). We then used mathematical modelling to quantify HCR signal profiles and compare
279 the two conditions (steady state and regeneration) in an unbiased manner. Previously, we
280 analysed cell cycle dynamics in the regenerating axolotl spinal cord using a piecewise model,
281 which assumes that zones of homogeneous behaviour are separated by sharp boundaries

282 (switch points) (Cura Costa et al., 2021; Rost et al., 2016). We reasoned that piecewise
283 modelling could similarly extract ‘gene expression level’ and ‘domain size’ from the HCR
284 data, with an attractive feature being that the switch point unambiguously determines the
285 gene expression boundary for further analyses (Figure S1a). We modelled *Msx1*, *Pax7*,
286 *Nkx6.1* and *Shh* using a 2-zone model, with the 2 zones representing ‘expression’ or
287 ‘background’. For *Pax6*, whose expression occurs centrally in the dorsal-ventral axis, we
288 used a 3-zone model (‘background’-‘expression’-‘background’) with two switch points
289 corresponding to the dorsal and ventral limits of *Pax6* expression. We performed individual
290 fitting of replicates (Supplementary Information), generated mean fittings (Figure 1e, Figure
291 S1b) and then used these to derive values for gene expression level and domain size (Table
292 2).

293 Piecewise modelling revealed a significant increase in the expression of all genes
294 assayed from steady state to regeneration, with a mean HCR signal increase ranging from
295 1.6-fold (*Shh*, *Nkx6.1*) to 2.2-fold (*Msx1*) (Figure 1f). The calculated switch points revealed
296 that the representation of dorsal-ventral progenitors contacting the spinal cord lumen changed
297 during regeneration. The dorsal gene domains became smaller (*Msx1*: -40.7%, *Pax7*: -
298 24.1%), the lateral *Pax6* domain remained the same size and the ventral gene domains
299 became larger (*Nkx6.1*: +14.4% and *Shh*: +84.5%) at 14 dpa compared to steady state (Figure
300 1g). Thus, this analysis suggested that the roof plate and floor plate signalling centres were
301 the domains that changed the most in their representation at the lumen. We confirmed the
302 increase in *Shh*+ floor plate size through an independent assay, immunostaining for SHH
303 protein at steady state and at 14 dpa (Figures S1c-d).

304 In summary, through mathematical modelling of HCR data, we determined that
305 axolotl spinal cord regeneration proceeds *via* significant increases in the expression level of
306 dorsal-ventral genes and a re-distribution of progenitor domains at the spinal cord lumen.
307 Notably, we found that the floor plate signalling centre increases in size during axolotl spinal
308 cord regeneration.

309

310 **Live labelling reveals changes in floor plate dynamics in the anterior-posterior axis.**

311 How do these dorsal-ventral changes relate to the anterior-posterior (snout-to-tail) axis of the
312 regenerating spinal cord, particularly in the region of injury-activated progenitor cells
313 (Albors et al., 2015; Cura Costa et al., 2021; Rost et al., 2016)? With the aim of resolving
314 such dynamics live during regeneration, we designed a dual reporter axolotl to co-visualise
315 dorsal cells and floor plate in which *Pax7* and *Shh* regulatory sequences controlled the
316 expression of mCherry and EGFP fluorescent proteins respectively.

317 We previously generated a *Pax7* knock-in axolotl that co-expresses membrane-
318 targeted mCherry and tamoxifen-inducible Cre recombinase from the *Pax7* locus
319 (“*Pax7^{mCherry-dERC}Cre*”, (Fei et al., 2017)). We used the same strategy to generate a *Shh* knock-
320 in axolotl that expresses membrane-targeted EGFP and tamoxifen-inducible Cre from the
321 *Shh* locus (“*Shh^{EGFP-dERC}Cre*”). We mated these axolotls together to generate germline-
322 transmitted dual reporter axolotls that simultaneously label *Pax7*⁺ and *Shh*⁺ cells with
323 distinct fluorophores (Figure 2a, top). Transgenic axolotls used in this work are listed in
324 Table 3.

325 Imaging dual reporter axolotls revealed restriction of mCherry and EGFP to opposite
326 sides of the spinal cord, suggesting correct labelling of dorsal and ventral progenitors (Figure
327 2a, bottom and Figure 2b). We demonstrated previously, and confirm here (Figure S2a), that
328 *Pax7*^{mCherry-dERC} faithfully recapitulates *Pax7* expression in the spinal cord and in tail muscle
329 (Fei et al., 2017). We similarly tested the fidelity of the *Shh* reporter by performing HCR
330 against *Shh* transcripts on *Shh*^{EGFP-dERC} spinal cord cross sections (Figure 2c). We found that
331 100% of EGFP+ cells expressed *Shh* transcripts ($n = 72$ cells from 6 spinal cords), although
332 not all *Shh*+ cells expressed EGFP (67.5 ± 14.0 % of *Shh*+ cells were EGFP+, Figure S2b).
333 The mean EGFP expression level was 2.1 times in regenerating tails compared to steady state
334 (Figures S2c-d), a magnitude consistent with our *Shh* HCR analyses (Figure 1f).

335 Having validated the dual reporter axolotls, we performed tail amputation and live
336 imaged the regenerating spinal cord every 2-3 days until 14 dpa (Figure 2d). We observed
337 fluorescence in the outgrowing spinal cord and, consistent with the fixed tissue data, mCherry
338 and EGFP appeared restricted to the dorsal and ventral sides (Figure 2e). Interestingly, this
339 time series revealed a transient and spatially restricted increase in *Shh*^{EGFP-dERC} signal
340 towards the spinal cord tip (also called ‘terminal vesicle’) (Figure 2e, insets). This high signal
341 zone was located more posteriorly in the spinal cord than the regions harvested for the HCR
342 analyses. Thus, we infer that, in addition to a general increase in *Shh* expression during
343 regeneration (Figure 1f), there is a posterior zone in which *Shh*^{EGFP} signal is particularly high.
344 This high signal could be the result of elevated *Shh* expression, a higher density of *Shh*+ cells,
345 or a combination of both. By measuring mean fluorescence intensity in outgrowing spinal
346 cords (Figure S2e), we found that this high *Shh*^{EGFP} signal zone extended ~800 μ m anteriorly
347 from the regenerating tip and was apparent at 6-8 dpa, before disappearing by day 14 (Figure

348 2f). An equivalent analysis of *Pax7^{mCherry-dERC}* revealed no such dynamics – and, in fact,
349 there was a tendency of decreasing expression towards the tail tip across all time points
350 (Figure 2g). In sum, we identified both anterior-posterior and dorsal-ventral changes in floor
351 plate dynamics during axolotl spinal cord regeneration.

352

353 ***Shh*+** cells selectively generate ***Shh*+** cells during spinal cord regeneration.

354 Given these spatiotemporal differences in floor plate behaviour, an important question is how
355 *Shh*+ cells contribute to the regenerating spinal cord. A simple model is that *Shh*+ cells give
356 rise only to *Shh*+ floor plate during regeneration. However, another possibility is that *Shh*+
357 floor plate can switch dorsal-ventral identity to give rise to other neural progenitors
358 (Mchedlishvili et al., 2007). To distinguish between these possibilities (fate-restricted model
359 vs. flexible identity model, Figure 3a), we used a genetic strategy to label *Shh*+ cells and
360 track their progeny during regeneration. We crossed *Shh*^{EGFP-dERC} axolotls, which express
361 tamoxifen-inducible Cre recombinase, to our previously published fate mapping axolotl
362 (*Caggs:loxP-Stop-loxP-mCherry*) (Figure 3b). Treating the progeny with 4-
363 hydroxytamoxifen (4-OHT) induces recombination and removal of the Stop cassette,
364 labelling *Shh*+ cells and their progeny permanently with mCherry.

365 Initially, we attempted lineage labelling at steady state by treating axolotls once or
366 three times with 2 μ M 4-OHT, but neither strategy induced mCherry labelling robustly
367 (Figure S3a), potentially due to low expression of *Shh* and *Cre* at steady state (Figures S2c-
368 d). Therefore, we treated animals with 4-OHT after tail amputation, which elevates *Shh*
369 expression (Figures S2c-d). By treating animals three times with 4-OHT from 7 dpa, we

370 succeeded in labelling sparse ventral cells in the spinal cord (“start of lineage tracing”)
371 (Figure S3a). Importantly, this labelling only occurred in 4-OHT treated animals (Figure
372 S3b). HCR for *Shh* mRNA revealed that almost 100% of mCherry-labelled cells were *Shh*+

373 ($n = 78/79$ cells from 15 tails) (Figure 3c). Notably, we labelled medial, medio-lateral and
374 lateral floor plate cells, allowing us to trace all regions of the floor plate (Figure 3c). Across
375 all samples, we observed only one single mCherry+ *Shh*-negative cell, demonstrating the
376 overall specificity of labelling (Figure S3c).

377 Having labelled *Shh*+ cells, we examined their lineage contributions to spinal cord
378 regeneration. We re-amputated labelled tails within a zone 500 μm posterior to mCherry+
379 cells (Figure S3d), as neural progenitors within this zone contribute to spinal cord
380 regeneration (Mchedlishvili et al., 2007). We harvested tails at 7 dpa (“short-term tracing”)
381 or 28 dpa (“long-term tracing”) (Figure 3d). As expected, we observed an increase in the
382 number of mCherry+ cells during the tracing window as they proliferated and contributed to
383 regeneration (Figure S3e). To identify the traced cells, we performed HCR against *Shh*. We
384 found that 100% of mCherry labelled cells expressed *Shh* mRNA both at 7 dpa (Figure 3e)
385 ($n = 53$ cells from 19 tails) and at 28 dpa (Figure 3f) ($n = 145$ cells from 8 tails), with little
386 change in the positions of the labelled cells within the floor plate (medial, medio-lateral or
387 lateral) (Figures 3c, e-f). These results support that *Shh*+ cells maintain floor plate identity
388 during axolotl spinal cord regeneration.

389 One risk with the lineage tracing was that we failed to label other progenitor cells due
390 to a lack of expression of the fate mapping cassette. To exclude this possibility, we analysed
391 spinal cord sections from *Caggs:loxP-GFP-loxP-mCherry* fate mapping axolotls (Khattak et
392 al., 2013). These axolotls use the same expression system as those used in our lineage tracings

393 but additionally express GFP in any cell that expresses the memory cassette (independent of
394 Cre/loxP recombination). We found that whenever a *Shh*⁺ cell expressed the memory
395 cassette, neighbouring (more dorsal) progenitors also expressed the memory cassette,
396 indicating the potential to become labelled ($n = 27/28$ sections analysed, harvested from 6
397 axolotls) (Figure S3f). On the other hand, we found that the most dorsal progenitors on the
398 other side of the spinal cord frequently lacked expression of the fate mapping cassette (Figure
399 S3f). This is an important consideration for investigations into dorsal cells.

400 As a result of the sparse labelling efficiency in these experiments, we could detect
401 that *Shh*⁺ cells change morphology during regeneration. At the 28 dpa time point, anterior
402 spinal cord regions (closer to the original amputation plane) had already regenerated neurons
403 while posterior regions (towards the outgrowing tip) still lacked neurons (Figure S3g). As
404 neurons are regenerated in an anterior-to-posterior direction, the anterior regions containing
405 neurons could be considered more ‘mature’ regenerate tissue compared to the more
406 ‘immature’ posterior regions lacking neurons. We found that *Shh*⁺ cells in the immature
407 spinal cord had a simple, trapezoid morphology, while *Shh*⁺ cells in the mature part had a
408 more complex shape including an apical process extending towards the spinal cord lumen
409 and one or more basal processes ventrally (Figure S3g). This morphological difference is
410 likely related to maturation state rather than anterior-posterior differences, as all labelled
411 *Shh*⁺ cells had the simpler morphology at the 7 dpa time point (Figure 3e). This is the first
412 time that the complex morphology of floor plate cells has been captured in regenerating
413 spinal cord.

414 Several injury paradigms are used to study mechanisms of spinal cord regeneration.
415 Spinal cord transection in zebrafish elevates dorsal-ventral patterning gene expression,

416 including *Shh*, local to the injury site (Reimer et al., 2009). In this study, by taking a
417 mathematical modelling approach to the axolotl model, we found that tail amputation triggers
418 not only a general increase in dorsal-ventral gene expression but also a larger floor plate and
419 a high *Shh*^{EGFP} zone within ~800 μ m of the regenerating spinal cord tip. The function of this
420 high *Shh*^{EGFP} zone, and if it relates to previous suggestions of a higher plasticity in progenitor
421 identity at the terminal vesicle (Mchedlishvili et al., 2007) are important topics for future
422 study. In both zebrafish and axolotls, upregulation of dorsal-ventral genes is observed by 14
423 days post-injury. It is possible that this upregulation reflects the acquisition of a more
424 development-like cellular state for regeneration. Interestingly, *Pax6* is upregulated after
425 spinal cord transection in rats concomitant with cell proliferation (Yamamoto et al., 2001),
426 suggesting the potential for similar (but more limited) molecular changes in mammals.

427 Although *Shh*⁺ cells persist in the axolotl spinal cord throughout life, their cellular
428 contributions to regeneration had not been identified. By performing genetic lineage tracing,
429 we found that *Shh*⁺ cells are limited to generating regeneration floor plate in the tail
430 amputation model. We were only able to label sparse *Shh*⁺ cells due to a poor efficiency of
431 Cre/loxP-mediated memory cassette recombination. It is likely that labelling efficiency could
432 be improved by increasing Cre activity (e.g. reducing the number of ER^{T2} domains fused to
433 the Cre recombinase) and/or increasing Cre expression level (e.g. expressing the Cre
434 recombinase prior to EGFP in the knock-in cassette). However, sparse labelling was powerful
435 for revealing floor plate cell morphology. Although floor plate cells are commonly described
436 to be cuboidal or trapezoid, they are thought to have a more complex morphology
437 characterised by apical and basal cellular processes (Campbell and Peterson, 1993;
438 Yaginuma et al., 1991). Recently, it was found that the basal processes of chick floor plate

439 cells comprise multiple extensions that enwrap the growth cones of dorsal commissural
440 neurons and constrain them to a straight trajectory path (Ducuing et al., 2020). Here, we
441 discovered that axolotl floor plate cells lack complex basal processes at 7 dpa but elaborate
442 these later during regeneration (by 28 dpa), possibly reflecting functional maturation. These
443 basal processes could serve an axon guidance function for regenerating axons, but this should
444 be tested functionally.

445 Previous experiments had suggested that neural progenitors can change dorsal-ventral
446 identity during axolotl regeneration (Mchedlishvili et al., 2007). Determining if *Shh*⁺ cells
447 are exceptions to this behaviour, or if their fate could be changed by external manipulation
448 or a different injury paradigm, are important future directions. Reciprocally, lineage tracing
449 the other neural progenitors in the spinal cord will reveal the degree to which these cells can
450 contribute to the formation of floor plate and roof plate signalling centres. During axolotl
451 limb regeneration, cells that did not previously express *Shh* can readily generate *Shh*⁺
452 signalling centre cells (Otsuki et al., 2023). Studying the origins and fate limitations of
453 signalling centres in different tissues will uncover different avenues to tissue patterning *in*
454 *vivo* and in tissue engineering applications.

455

456 **Author contributions**

457 L.I.A. designed experiments, performed all experiments, analysed data and wrote the
458 manuscript. E.C.C. analysed data and wrote the manuscript. O.C. secured funding, analysed
459 data and wrote the manuscript. L.O. conceived the project, secured funding, designed
460 experiments, generated transgenic axolotls, analysed data, supervised the project and wrote
461 the manuscript. E.M.T. conceived the project, secured funding, supervised the project and
462 wrote the manuscript. All authors approved the manuscript.

463 **Acknowledgements**

464 We thank Tanaka laboratory members for reagents (Hannah Stuart, Wouter Masselink,
465 Anastasia Polikarpova, Pietro Tardivo) and project discussions (Elad Bassat, Katharina Lust,
466 Hannah Stuart). We are grateful to the caretaker team (Magdalena Blaschek, Emina Silic,
467 Victoria Szilagyi, Andrea Lentz-Koblenc, Veronika Vojnicsek) for excellent axolotl care and
468 the Molecular Biology Service and BioOptics facility at IMP/IMBA for expert support.

469 E.C.C. and O.C. were funded by a PICT-2019-03828 grant from AGENCIA (National
470 Agency from the Promotion of Research, Technological Development and Innovation,
471 Argentina). L.O. was funded by fellowship LT000785/2019-L from HFSP (Human Frontier
472 Science Program). L.I.A. and E.M.T. were funded by Advanced Grant 742046
473 (RegGeneMems) from the ERC (European Research Council) and Special Research Program
474 of the Austrian Science Fund (FWF) Project F78. For the purpose of open access, the authors
475 have applied a CC BY public copyright licence to any Author Accepted Manuscript version
476 arising from this submission.

477 **References**

478

479 **Albors, A. R., Tazaki, A., Rost, F., Nowoshilow, S., Chara, O. and Tanaka, E. M.**
480 (2015). Planar cell polarity-mediated induction of neural stem cell expansion during
481 axolotl spinal cord regeneration. *Elife* **4**, 664.

482 **Albors, A. R., Singer, G. A., Llorens-Bobadilla, E., Frisén, J., May, A. P., Ponting, C.**
483 **P. and Storey, K. G.** (2023). An ependymal cell census identifies heterogeneous and
484 ongoing cell maturation in the adult mouse spinal cord that changes dynamically on
485 injury. *Dev. Cell* **58**, 239-255.e10.

486 **Becker, T., Wullimann, M. F., Becker, C. G., Bernhardt, R. R. and Schachner, M.**
487 (1997). Axonal regrowth after spinal cord transection in adult zebrafish. *J. Comp.*
488 *Neurol.* **377**, 577-595.

489 **Briscoe, J., Pierani, A., Jessell, T. M. and Ericson, J.** (2000). A Homeodomain Protein
490 Code Specifies Progenitor Cell Identity and Neuronal Fate in the Ventral Neural Tube.
491 *Cell* **101**, 435-445.

492 **Campbell, R. M. and Peterson, A. C.** (1993). Expression of a lacZ transgene reveals floor
493 plate cell morphology and macromolecular transfer to commissural axons. *Development*
494 **119**, 1217-1228.

495 **Cañizares, M. A., Albors, A. R., Singer, G., Suttie, N., Gorkic, M., Felts, P. and Storey,**
496 **K. G.** (2020). Multiple steps characterise ventricular layer attrition to form the
497 ependymal cell lining of the adult mouse spinal cord central canal. *J. Anat.* **236**, 334-
498 350.

499 **Choi, H. M. T., Schwarzkopf, M., Fornace, M. E., Acharya, A., Artavanis, G.,**
500 **Stegmaier, J., Cunha, A. and Pierce, N. A.** (2018). Third-generation in
501 situhybridization chain reaction: multiplexed, quantitative, sensitive, versatile, robust.
502 *Development* **145**,

503 **Cura Costa, E., Otsuki, L., Albors, A. R., Tanaka, E. M. and Chara, O.** (2021).
504 Spatiotemporal control of cell cycle acceleration during axolotl spinal cord regeneration.
505 *Elife* **10**,

506 **Cura Costa, E. and Chara, O.** (2024). Jupyter notebooks for: Lineage tracing of shh+
507 floor plate cells and dynamics of dorsal-ventral gene expression in the regenerating
508 axolotl spinal cord (v1.0.0). *Zenodo*. doi:10.5281/zenodo.11520810.

509 **Ducuing, H., Gardette, T., Pignata, A., Kindbeiter, K., Bozon, M., Thoumine, O.,**
510 **Delloye-Bourgeois, C., Tauszig-Delamasure, S. and Castellani, V.** (2020). SlitC-

511 PlexinA1 mediates iterative inhibition for orderly passage of spinal commissural axons
512 through the floor plate. *eLife* **9**, e63205.

513 **Echelard, Y., Epstein, D. J., St-Jacques, B., Shen, L., Mohler, J., McMahon, J. A. and**
514 **McMahon, A. P.** (1993). Sonic hedgehog, a member of a family of putative signaling
515 molecules, is implicated in the regulation of CNS polarity. *Cell* **75**, 1417–1430.

516 **Egar, M. and Singer, M.** (1972). The role of ependyma in spinal cord regeneration in the
517 urodele, Triturus. *Exp. Neurol.* **37**, 422–430.

518 **Fei, J.-F., Schuez, M., Knapp, D., Taniguchi, Y., Drechsel, D. N. and Tanaka, E. M.**
519 (2017). Efficient gene knockin in axolotl and its use to test the role of satellite cells in
520 limb regeneration. *Proc. Natl. Acad. Sci.* **114**, 12501–12506.

521 **Fei, J.-F., Lou, W. P.-K., Knapp, D., Murawala, P., Gerber, T., Taniguchi, Y.,**
522 **Nowoshilow, S., Khattak, S. and Tanaka, E. M.** (2018). Application and optimization
523 of CRISPR-Cas9-mediated genome engineering in axolotl (*Ambystoma mexicanum*).
524 *Nat Protoc* **13**, 2908–2943.

525 **Ghazale, H., Ripoll, C., Leventoux, N., Jacob, L., Azar, S., Mamaeva, D., Glasson, Y.,**
526 **Calvo, C.-F., Thomas, J.-L., Meneceur, S., et al.** (2019). RNA Profiling of the Human
527 and Mouse Spinal Cord Stem Cell Niches Reveals an Embryonic-like Regionalization
528 with MSX1+ Roof-Plate-Derived Cells. *Stem Cell Rep.* **12**, 1159–1177.

529 **Harris, C. R., Millman, K. J., Walt, S. J. van der, Gommers, R., Virtanen, P.,**
530 **Cournapeau, D., Wieser, E., Taylor, J., Berg, S., Smith, N. J., et al.** (2020). Array
531 programming with NumPy. *Nature* **585**, 357–362.

532 **Hui, S. P., Dutta, A. and Ghosh, S.** (2010). Cellular response after crush injury in adult
533 zebrafish spinal cord. *Dev. Dyn.* **239**, 2962–2979.

534 **Hunter, J. D.** (2007). Matplotlib: A 2D Graphics Environment. *Comput. Sci. Eng.* **9**, 90–
535 95.

536 **Joksimovic, M., Patel, M., Taketo, M. M., Johnson, R. and Awatramani, R.** (2012).
537 Ectopic Wnt/Beta-Catenin Signaling Induces Neurogenesis in the Spinal Cord and
538 Hindbrain Floor Plate. *PLoS ONE* **7**, e30266.

539 **Kawaguchi, A., Wang, J., Knapp, D., Murawala, P., Nowoshilow, S., Masselink, W.,**
540 **Taniguchi-Sugiura, Y., Fei, J.-F. and Tanaka, E. M.** (2024). A chromatin code for
541 limb segment identity in axolotl limb regeneration. *Dev. Cell*.

542 **Khattak, S., Schuez, M., Richter, T., Knapp, D., Haigo, S. L., Sandoval-Guzmán, T.,**
543 **Hradlikova, K., Duemmler, A., Kerney, R. and Tanaka, E. M.** (2013). Germline
544 Transgenic Methods for Tracking Cells and Testing Gene Function during Regeneration
545 in the Axolotl. *Stem Cell Rep.* **1**, 90–103.

546 **Khattak, S., Murawala, P., Andreas, H., Kappert, V., Schuez, M., Sandoval-Guzmán,
547 T., Crawford, K. and Tanaka, E. M.** (2014). Optimized axolotl (*Ambystoma
548 mexicanum*) husbandry, breeding, metamorphosis, transgenesis and tamoxifen-mediated
549 recombination. *Nat. Protoc.* **9**, 529–540.

550 **Liem, K. F., Tremml, G. and Jessell, T. M.** (1997). A Role for the Roof Plate and Its
551 Resident TGF β -Related Proteins in Neuronal Patterning in the Dorsal Spinal Cord. *Cell*
552 **91**, 127–138.

553 **Mchedlishvili, L., Epperlein, H. H., Telzerow, A. and Tanaka, E. M.** (2007). A clonal
554 analysis of neural progenitors during axolotl spinal cord regeneration reveals evidence
555 for both spatially restricted and multipotent progenitors. *Development* **134**, 2083–2093.

556 **Meletis, K., Barnabé-Heider, F., Carlén, M., Evergren, E., Tomilin, N., Shupliakov, O.
557 and Frisén, J.** (2008). Spinal Cord Injury Reveals Multilineage Differentiation of
558 Ependymal Cells. *PLoS Biol.* **6**, e182.

559 **Muroyama, Y., Fujihara, M., Ikeya, M., Kondoh, H. and Takada, S.** (2002). Wnt
560 signaling plays an essential role in neuronal specification of the dorsal spinal cord.
561 *Genes Dev.* **16**, 548–553.

562 **Nowoshilow, S., Fei, J.-F., Voss, R. S., Tanaka, E. M. and Murawala, P.** (2021). Gene
563 and transgenics nomenclature for the laboratory axolotl - *Ambystoma mexicanum*. *Dev.
564 Dyn.*

565 **Otsuki, L., Plattner, S. A., Taniguchi-Sugiura, Y. and Tanaka, E. M.** (2023). Molecular
566 basis for positional memory and its reprogrammability in limb regeneration. *bioRxiv*.

567 **Piatt, J.** (1955). Regeneration of the spinal cord in the salamander. *J. Exp. Zool.* **129**, 177–
568 207.

569 **Qiu, M., Shimamura, K., Sussel, L., Chen, S. and Rubenstein, J. L. R.** (1998). Control
570 of anteroposterior and dorsoventral domains of Nkx-6.1 gene expression relative to
571 other Nkx genes during vertebrate CNS development. *Mech. Dev.* **72**, 77–88.

572 **Reimer, M. M., Kuscha, V., Wyatt, C., Sörensen, I., Frank, R. E., Knüwer, M.,
573 Becker, T. and Becker, C. G.** (2009). Sonic Hedgehog Is a Polarized Signal for Motor
574 Neuron Regeneration in Adult Zebrafish. *J. Neurosci.* **29**, 15073–15082.

575 **Rost, F., Albors, A. R., Mazurov, V., Brusch, L., Deutsch, A., Tanaka, E. M. and
576 Chara, O.** (2016). Accelerated cell divisions drive the outgrowth of the regenerating
577 spinal cord in axolotls. *Elife* **5**, 516.

578 **Sagner, A. and Briscoe, J.** (2019). Establishing neuronal diversity in the spinal cord: a
579 time and a place. *Development* **146**, dev182154.

580 **Sander, M., Paydar, S., Ericson, J., Briscoe, J., Berber, E., German, M., Jessell, T. M.**
581 **and Rubenstein, J. L. R.** (2000). Ventral neural patterning by Nkx homeobox genes:
582 Nkx6.1 controls somatic motor neuron and ventral interneuron fates. *Genes Dev.* **14**,
583 2134–2139.

584 **Schindelin, J., Arganda-Carreras, I., Frise, E., Kaynig, V., Longair, M., Pietzsch, T.,**
585 **Preibisch, S., Rueden, C., Saalfeld, S., Schmid, B., et al.** (2012). Fiji: an open-source
586 platform for biological-image analysis. *Nat. Methods* **9**, 676–682.

587 **Schloissnig, S., Kawaguchi, A., Nowoshilow, S., Falcon, F., Otsuki, L., Tardivo, P.,**
588 **Timoshevskaya, N., Keinath, M. C., Smith, J. J., Voss, S. R., et al.** (2021). The giant
589 axolotl genome uncovers the evolution, scaling, and transcriptional control of complex
590 gene loci. *Proc. Natl. Acad. Sci. U.S.A.* **118**,

591 **Schnapp, E., Kragl, M., Rubin, L. and Tanaka, E. M.** (2005). Hedgehog signaling
592 controls dorsoventral patterning, blastema cell proliferation and cartilage induction
593 during axolotl tail regeneration. *Development* **132**, 3243–3253.

594 **Sun, A. X., Londono, R., Hudnall, M. L., Tuan, R. S. and Lozito, T. P.** (2018).
595 Differences in neural stem cell identity and differentiation capacity drive divergent
596 regenerative outcomes in lizards and salamanders. *Proc. Natl. Acad. Sci. U.S.A.* **115**,
597 E8256–E8265.

598 **Thygesen, M. M., Lauridsen, H., Pedersen, M., Orlowski, D., Mikkelsen, T. W. and**
599 **Rasmussen, M. M.** (2019). A clinically relevant blunt spinal cord injury model in the
600 regeneration competent axolotl (*Ambystoma mexicanum*) tail. *Exp. Ther. Med.* **17**,
601 2322–2328.

602 **Virtanen, P., Gommers, R., Oliphant, T. E., Haberland, M., Reddy, T., Cournapeau,**
603 **D., Burovski, E., Peterson, P., Weckesser, W., Bright, J., et al.** (2020). SciPy 1.0:
604 fundamental algorithms for scientific computing in Python. *Nat. Methods* **17**, 261–272.

605 **Walker, S., Santos-Ferreira, T. and Echeverri, K.** (2023). A Reproducible Spinal Cord
606 Crush Injury in the Regeneration-Permissive Axolotl. *Methods Mol. Biol. (Clifton, NJ)*
607 **2636**, 237–246.

608 **Waskom, M.** (2021). seaborn: statistical data visualization. *J. Open Source Softw.* **6**, 3021.

609 **Yaginuma, H., Homma, S., Künzi, R. and Oppenheim, R. W.** (1991). Pathfinding by
610 growth cones of commissural interneurons in the chick embryo spinal cord: A light and
611 electron microscopic study. *J. Comp. Neurol.* **304**, 78–102.

612 **Yamamoto, S., Nagao, M., Sugimori, M., Kosako, H., Nakatomi, H., Yamamoto, N.,**
613 **Takebayashi, H., Nabeshima, Y., Kitamura, T., Weinmaster, G., et al.** (2001).
614 Transcription Factor Expression and Notch-Dependent Regulation of Neural Progenitors
615 in the Adult Rat Spinal Cord. *J. Neurosci.* **21**, 9814–9823.

617 **Tables**

618 **Table 1. Samples quantified for mathematical modelling of HCR *in situ* staining.**

619 All quantifications were performed on maximum intensity projections of 20 μm thick spinal
620 cord cross-sections. $n = 6$ axolotls for each of steady state and 14 dpa.

Gene	Condition	Number of sections quantified
<i>Msx1</i>	Steady state	30
	14 dpa blastema	36
<i>Pax7</i>	Steady state	22
	14 dpa blastema	38
<i>Pax6</i>	Steady state	36
	14 dpa blastema	43
<i>Nkx6.1</i>	Steady state	36
	14 dpa blastema	43
<i>Shh</i>	Steady state	22
	14 dpa blastema	38

621

622 **Table 2. Mean HCR signal and domain sizes calculated by the piecewise model.**

623 Mean HCR signal is after correction by subtracting background fluorescence.

Gene	Condition	Piecewise model	
		Mean HCR signal* $\pm SD$	Mean domain size $\pm SD$
<i>Msx1</i>	Steady state	25.5 ± 12.4	15.2 ± 10.3
	14 dpa	55.5 ± 41.0	9.0 ± 3.6

<i>Pax7</i>	Steady state	146.0 ± 88.7	33.5 ± 8.9
	14 dpa	255.3 ± 117.5	25.4 ± 9.9
<i>Pax6</i>	Steady state	60.4 ± 24.8	36.9 ± 15.3
	14 dpa	109.8 ± 39.9	34.0 ± 12.6
<i>Nkx6.1</i>	Steady state	79.8 ± 37.0	47.1 ± 14.3
	14 dpa	126.5 ± 61.1	53.9 ± 12.2
<i>Shh</i>	Steady state	85.6 ± 46.8	11.5 ± 8.2
	14 dpa	135.8 ± 6.3	21.1 ± 8.8

624

625 **Table 3. Transgenic axolotls used in this study.**

Simple name	Genotype	Reference	Used in Figures
<i>d/d</i>	<i>d/d</i>	-	1a-g; S1a-d
<i>Shh</i> ^{EGFP-dERCre}	tm(<i>Shh</i> ^{v/+} ; <i>Shh</i> -P2A- <i>myr-EGFP</i> -T2A- <i>ER</i> ^{T2} - <i>Cre-ER</i> ^{T2}) ^{Etnka}	this study	2a-g; 3b-f; S2b-e, S3a-e, g
<i>Pax7</i> ^{mCherry-dERCre}	tm(<i>Pax7</i> ^{v/+} ; <i>Pax7</i> -P2A- <i>memCherry</i> -T2A- <i>ER</i> ^{T2} - <i>Cre-ER</i> ^{T2}) ^{Etnka}	(Fei et al., 2017)	2a-b, 2d-g; S2a
Fate mapping axolotl (Stop-loxP-mCherry)	tgSceI(<i>Caggs:loxP-GFP-dead(Stop)-loxP-mCherry</i>) ^{Etnka}	(Kawaguchi et al., 2024)	3b-f; S3a-e, g
Fate mapping axolotl (GFP-loxP-mCherry)	tgSceI(<i>Caggs:loxP-GFP-loxP-mCherry</i>) ^{Etnka}	(Khattak et al., 2013)	S3f

626

627 **Figure legends**

628 **Figure 1. Mathematical modelling of dorsal-ventral gene expression during axolotl**
629 **spinal cord regeneration.**

630 (a) Cross sections of steady state axolotl spinal cord, immunostained for neural progenitor
631 gene (SOX2), dorsal-ventral transcription factors (PAX7, PAX6) or floor plate signal (SHH).
632 DAPI labels nuclei. Maximum intensity projections through 20 μm of tissue, acquired with
633 confocal microscopy. Dorsal is up and ventral is down.

634 (b) Harvesting of steady state and 14 dpa regenerating spinal cord. Gray box indicates
635 approximate analysis area.

636 (c) Cross sections of spinal cords at steady state (top row) or 14 dpa (bottom row), stained
637 using HCR for mRNA encoding dorsal-ventral patterning genes (*Msx1*, *Pax7*, *Pax6*, *Nkx6.1*,
638 *Shh*) or neural progenitor gene *Sox2*. DAPI labels nuclei. Maximum intensity projections
639 through 20 μm of tissue, acquired with confocal microscopy.

640 (d) Fluorescence intensity plots for HCR data at steady state and 14 dpa. *x*-axis is normalised
641 distance along the dorsal-ventral (DV) axis, from dorsal to ventral. *y*-axis is HCR signal
642 intensity (measured gray values), which was measured by using the segmented line tool (Fiji)
643 to draw a line of thickness 100 through the neural progenitor layer of the spinal cord and
644 using the Measurement function. *n* numbers are given in Table 1.

645 (e) Plots depicting the fits of the piecewise models to the HCR data at steady state and 14
646 dpa. Solid lines and ribbons indicate mean HCR fluorescence measurements. Dotted lines
647 indicate the mean fit of the piecewise model. Orange line indicates the switch point \pm SD.

648 (f) Box plots comparing the expression levels of dorsal-ventral genes at steady state and 14
649 dpa, as determined by piecewise modelling. Dots indicate values from individually fitted
650 replicates. “Corrected HCR signal” is HCR signal intensity minus background intensity. ***:
651 $p < 0.05$, Mann-Whitney U tests. Exact p values: *Msx1* (1.35×10^{-4}), *Pax7* (3.40×10^{-4}), *Pax6*
652 (3.44×10^{-8}), *Nkx6.1* (6.84×10^{-5}), *Shh* (4.31×10^{-4}).

653 (g) Box plots comparing dorsal-ventral domain sizes at the lumen at steady state and 14 dpa,
654 as determined by piecewise modelling. Dots indicate values from individually fitted
655 replicates. Statistical comparison was performed by Mann-Whitney U tests. Exact p values:
656 *Msx1* (2.08×10^{-4}), *Pax7* (3.07×10^{-3}), *Pax6* (ns), *Nkx6.1* (2.77×10^{-2}), *Shh* (1.76×10^{-4}).

657

658 **Figure 2. Live tracking of a dorsal-ventral reporter axolotl reveals a high *Shh* upregulation
659 zone during regeneration.**

660 (a) A dual transgenic axolotl to track dorsal-ventral gene expression in axolotl spinal cord.
661 CRISPR/Cas9-mediated knock-in results in co-expression of mCherry and tamoxifen-
662 inducible Cre from the *Pax7* locus (Fei et al., 2017) or EGFP and tamoxifen-inducible Cre
663 from the *Shh* locus (this study). Dual transgenics are heterozygous for each allele. A lateral
664 view of a 2 cm axolotl reveals mCherry and EGFP expression on the dorsal and ventral sides
665 of the spinal cord respectively. Additional expression is seen in muscle cell lineages
666 (mCherry) and the cartilage rod (EGFP).

667 (b) Spinal cord cross section from a 5 cm dual transgenic axolotl at 14 dpa. Red and cyan
668 depict endogenous *Pax7*^{*mCherry-dERC*^{Cre}} and *Shh*^{*EGFP-dERC*^{Cre}} fluorescence. DAPI labels nuclei.

669 Asterisk indicates autofluorescence. Maximum intensity projection through 20 μ m of tissue,
670 acquired with confocal microscopy.

671 (c) Spinal cord cross section from a 5 cm dual transgenic axolotl at 14 dpa. *Pax7mCherry-dERCre*
672 is not depicted. Cyan depicts endogenous *Shh*^{EGFP-dERCre} fluorescence. Magenta is HCR
673 labelling against endogenous *Shh* mRNA. 100% of *Shh*^{EGFP-dERCre}+ cells were *Shh* mRNA+
674 ($n = 72$ cells from 6 spinal cords). Asterisk indicates autofluorescence. Maximum intensity
675 projection through 20 μ m of tissue, acquired with confocal microscopy.

676 (d) An amputation-regeneration time course to measure changes in *Pax7mCherry-dERCre* and
677 *Shh*^{EGFP-dERCre} expression. Boxed areas represent images areas in (e).

678 (e) Widefield microscopy of regenerating tails from 3 cm axolotls. Insets are magnifications
679 of the regenerating spinal cord tip. Asterisks indicate the amputated tip of the cartilage rod,
680 which acts as an indicator of the amputation plane.

681 (f) Quantification of *Shh*^{EGFP-dERCre} fluorescent signal in the regenerating part of the spinal
682 cord. Dark lines are mean intensity values averaged from $n = 6$ spinal cords per time point;
683 pale lines indicate standard deviations.

684 (g) Quantification of *Pax7mCherry-dERCre* fluorescent signal in the regenerating part of the spinal
685 cord. Dark lines are mean intensity values averaged from $n = 6$ spinal cords per time point;
686 pale lines indicate standard deviations.

687

688 **Figure 3. *Shh*+ cells give rise to *Shh*+ cells during spinal cord regeneration.**

689 (a) Two hypotheses for how *Shh*⁺ cells contribute to spinal cord regeneration.

690 (b) Genetic strategy to lineage trace *Shh*⁺ cells. *Shh*⁺ cells continuously express tamoxifen-
691 inducible Cre. Pulse application of 4-OHT induces Cre translocation to the nucleus, where it
692 excises the STOP sequence in the fate mapping cassette by Cre/loxP recombination. This
693 results in permanent expression of mCherry in the *Shh*⁺ cell and its progeny.

694 (c) Spinal cord cross sections from *Shh* lineage tracing axolotls pulsed three times with 4-
695 OHT. 98.7% of mCherry cells express *Shh* mRNA ($n = 78/79$ cells, from 15 tails). Cells were
696 labelled in all regions (medial, medio-lateral, lateral) of the floor plate. DAPI labels nuclei.
697 Maximum intensity projections through 20 μm of tissue, acquired with confocal microscopy.

698 (d) Amputation-regeneration time course to lineage trace *Shh*⁺ cells. *Shh*⁺ cells were labelled
699 with mCherry as in (c), then spinal cords were re-amputated within 500 μm of labelled cells
700 to induce them to contribute to regeneration. Replicate spinal cords were harvested at 7 dpa
701 (short-term tracing) and 28 dpa (long-term tracing) to assess lineage contributions.

702 (e) Spinal cord cross sections harvested from *Shh* lineage tracing axolotls at 7 dpa (short-
703 term tracing). 100% of mCherry cells expressed *Shh* mRNA ($n = 53$ cells from 19 spinal
704 cords). Labelled cells were seen in all regions of the floor plate. DAPI labels nuclei. Asterisk
705 indicates autofluorescence. Maximum intensity projections through 20 μm of tissue, acquired
706 with confocal microscopy.

707 (f) Spinal cord cross sections harvested from *Shh* lineage tracing axolotls at 28 dpa (long-
708 term tracing). 100% of mCherry cells express *Shh* mRNA ($n = 145$ cells from 8 spinal cords).

709 Labelled cells were seen in all regions of the floor plate. DAPI labels nuclei. Maximum
710 intensity projections through 20 μm of tissue, acquired with confocal microscopy.

711

712 **Figure S1. Quantification of changes in dorsal-ventral patterning gene expression**
713 **during regeneration.**

714 (a) Schematic depicting how the fit and switch point of piecewise modelling relate to gene
715 expression level and domain size determination.

716 (b) Piecewise modelling of HCR fluorescence data. For each gene, the steady state fit is
717 plotted with a solid gray line and 14 dpa fit with a solid green line. Individual fits to replicates
718 are plotted with dotted lines.

719 (c) Spinal cord cross sections at steady state and 14 dpa, immunostained for SHH. DAPI
720 labels nuclei. Asterisk indicates autofluorescence. Maximum intensity projections through
721 20 μm of tissue, acquired with confocal microscopy.

722 (d) Box plots showing the number of SHH+ cells at steady state and 14 dpa, as assessed by
723 antibody staining. ****: $p = 1.79 \times 10^{-9}$, Kolmogorov-Smirnov test, $n = 30$ cross sections
724 quantified per time point, harvested from 6 tails each.

725

726 **Figure S2. Characterisation of *Pax7*^{mCherry-dERC}-*Shh*^{EGFP-dERC} dual transgenic axolotl.**

727 (a) Spinal cord cross section from a 4 cm dual transgenic axolotl at 14 dpa. *Shh*^{EGFP-dERC} is
728 not depicted. Red depicts endogenous *Pax7*^{mCherry-dERC} fluorescence. Yellow is HCR

729 staining against *Pax7* mRNA. Maximum intensity projection through 20 μm of tissue,
730 acquired with confocal microscopy.

731 (b) Box plots depicting the fidelity of the *Shh*^{EGFP-dERC} reporter, as assessed in spinal cords
732 at 14 dpa. Specificity: the percentage of *Shh*^{EGFP-dERC} cells that express *Shh* mRNA
733 (assessed by HCR). Efficiency: the percentage of *Shh* mRNA-expressing cells that are
734 positive for *Shh*^{EGFP-dERC}. $n = 10$ spinal cords.

735 (c) Box plots depicting the signal intensity of the *Shh*^{EGFP-dERC} reporter in the floor plate at
736 steady state *vs* 14 dpa. ****: $p = 1.58 \times 10^{-11}$, unpaired *t*-test with Welch's correction. $n = 23$
737 sections analysed per time point.

738 (d) Spinal cord cross sections from 4 cm dual transgenic axolotls at steady state (left) or at
739 14 dpa (right). Images are displayed with the same intensity settings. *Pax7*^{mCherry-dERC} is not
740 depicted. Cyan is *Shh*^{EGFP-dERC} fluorescence. Magenta is HCR labelling against *Shh* mRNA
741 (floor plate). *Shh*^{EGFP-dERC} expression is weaker at steady state than during regeneration.
742 Maximum intensity projection through 20 μm of tissue, acquired with confocal microscopy.

743 (e) Strategy to quantify dual reporter fluorescence in the regenerating spinal cord. The
744 segmented line tool (Fiji) was used to draw a line of thickness 10 through the outgrowing
745 spinal cord from anterior to posterior, starting at the amputation plane (determined by the
746 cartilage rod stump). The Measurement function was used to extract mCherry and EGFP
747 fluorescence intensity as a continuous variable.

748

749 **Figure S3. Details of *Shh* lineage tracing experiment.**

750 (a) Induction of mCherry expression from the fate mapping cassette after different 4-OHT
751 treatment conditions. Three overnight pulses of 4-OHT treatment from 7 dpa was the only
752 condition that resulted in reliable mCherry labelling. In all experiments, approximately half
753 of the animals would have inherited the memory cassette from the parent, resulting in a
754 theoretical maximal labelling efficiency of ~50%.

755 (b) Lateral widefield image of a *Shh* lineage tracing axolotl prior to 4-OHT treatment. As
756 expected, no mCherry labelling is present, while *Shh*^{EGFP-dERC^{Cre}} expression (cyan) can be seen
757 in ventral cells.

758 (c) One single *Shh* negative cell labelled with mCherry (circled and arrowed) was observed
759 in the “start of tracing” cohort (total 79 cells). Yellow is HCR against *Shh* mRNA. DAPI
760 labels nuclei. Asterisk indicates autofluorescence.

761 (d) Lineage tracing was initiated by re-amputating 4-OHT-treated tails within a 500 µm zone
762 posterior to mCherry-labelled cells (most posterior cell is arrowed in two examples).

763 (e) Lateral widefield images depicting expansion of mCherry-labelled cell clones in the
764 spinal cord from 0 dpa to 28 dpa (long-term trace).

765 (f) Confirmation that the fate mapping cassette expresses in multiple domains of the spinal
766 cord. Spinal cord cross section harvested from 3 cm *Caggs:loxP-GFP-loxP-mCherry*
767 axolotls (Khattak et al., 2013) at 7 dpa. Green/gray is endogenous GFP (indicating fate
768 mapping cassette expression). Whenever *Shh*⁺ cells (magenta) expressed the fate mapping
769 cassette, adjacent spatial domains also expressed the cassette ($n = 27$ of 28 spinal cord

770 sections). Maximum intensity projection through 20 μm of tissue, acquired with confocal
771 microscopy.

772 (g) Examples of mCherry-labelled *Shh*⁺ cells at 28 dpa, located in the more mature part of
773 the regenerate (indicated by the presence of peripheral neurons) or in the more immature part
774 of the regenerate (indicated by lack of peripheral neurons and a small spinal cord diameter).
775 Some *Shh*⁺ cells in the mature regenerate extended one or more protrusions from their ventral
776 side, oriented laterally or directly away from the lumen (detected in 13/26 sections). Although
777 *Shh*⁺ cells in the immature part of the regenerate also extended lateral processes (see
778 Example 2), these were not as numerous as those in the mature part, and were not oriented
779 away from the lumen (representative of 56 sections).

780

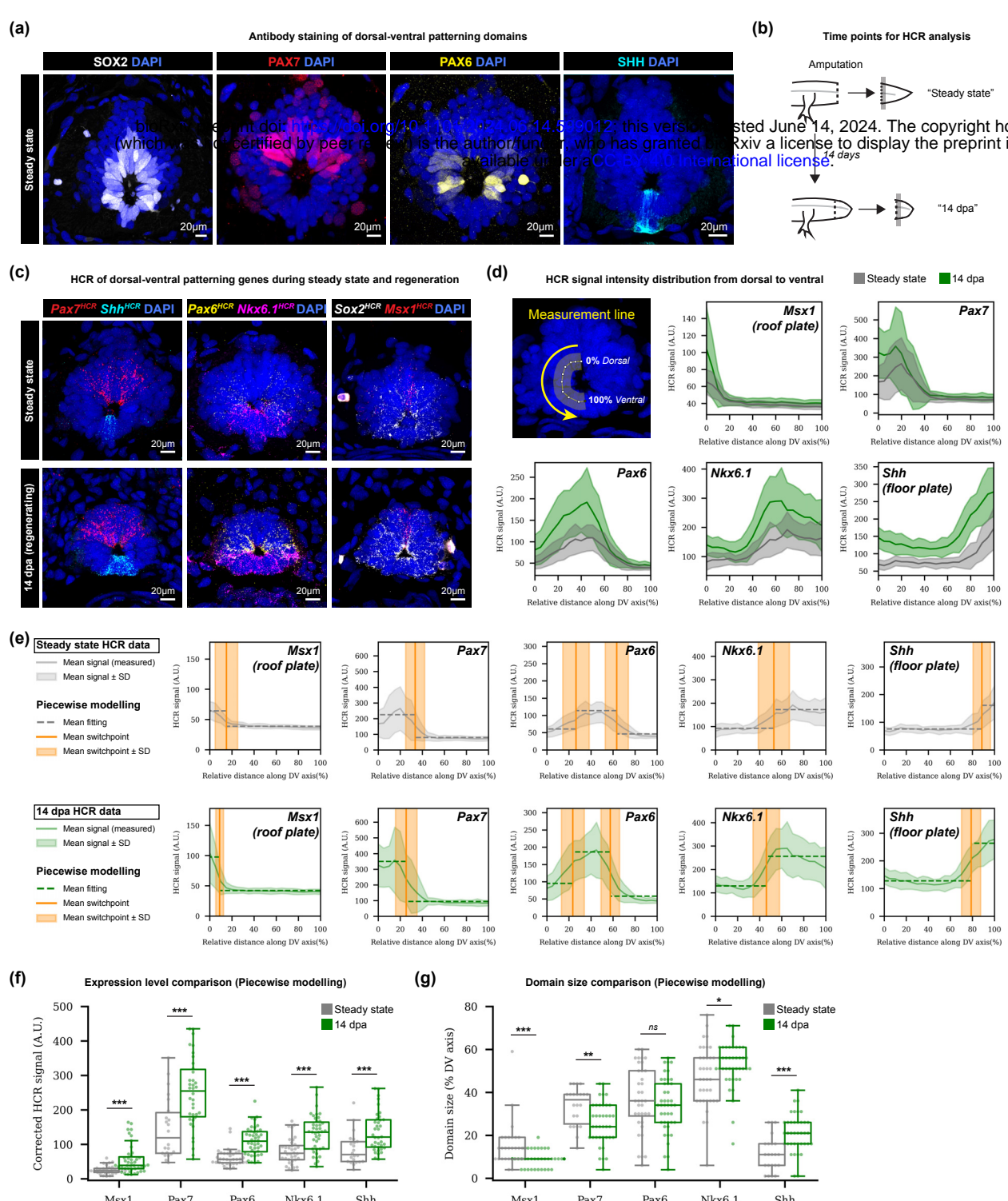


Figure 1. Mathematical modelling of dorsal-ventral gene expression during axolotl spinal cord regeneration.

(a) Cross sections of steady state axolotl spinal cord, immunostained for neural progenitor gene (SOX2), dorsal-ventral transcription factors (PAX7, PAX6) or floor plate signal (SHH). DAPI labels nuclei. Maximum intensity projections through 20 μm of tissue, acquired with confocal microscopy. Dorsal is up and ventral is down.

(b) Harvesting of steady state and 14 dpa regenerating spinal cord. Gray box indicates approximate analysis area.

(c) Cross sections of spinal cords at steady state (top row) or 14 dpa (bottom row), stained using HCR for mRNA encoding dorsal-ventral patterning genes (Msx1, Pax7, Pax6, Nkx6.1, Shh) or neural progenitor gene Sox2. DAPI labels nuclei. Maximum intensity projections through 20 μm of tissue, acquired with confocal microscopy.

(d) Fluorescence intensity plots for HCR data at steady state and 14 dpa. x-axis is normalised distance along the dorsal-ventral (DV) axis, from dorsal to ventral. y-axis is HCR signal intensity (measured gray values), which was measured by using the segmented line tool (Fiji) to draw a line of thickness 100 through the neural progenitor layer of the spinal cord and using the Measurement function. n numbers are given in Table 1.

(e) Plots depicting the fits of the piecewise models to the HCR data at steady state and 14 dpa. Solid lines and ribbons indicate mean HCR fluorescence measurements. Dotted lines indicate the mean fit of the piecewise model. Orange line indicates the switch point ± SD.

(f) Box plots comparing the expression levels of dorsal-ventral genes at steady state and 14 dpa, as determined by piecewise modelling. Dots indicate values from individually fitted replicates. "Corrected HCR signal" is HCR signal intensity minus background intensity. ***: $p < 0.05$, Mann-Whitney U tests. Exact p values: Msx1 (1.35×10^{-4}), Pax7 (3.40×10^{-4}), Pax6 (3.44×10^{-8}), Nkx6.1 (6.84×10^{-5}), Shh (4.31×10^{-4}).

(g) Box plots comparing dorsal-ventral domain sizes at the lumen at steady state and 14 dpa, as determined by piecewise modelling. Dots indicate values from individually fitted replicates. Statistical comparison was performed by Mann-Whitney U tests. Exact p values: Msx1 (2.08×10^{-4}), Pax7 (3.07×10^{-3}), Pax6 (ns), Nkx6.1 (2.77×10^{-2}), Shh (1.76×10^{-4}).

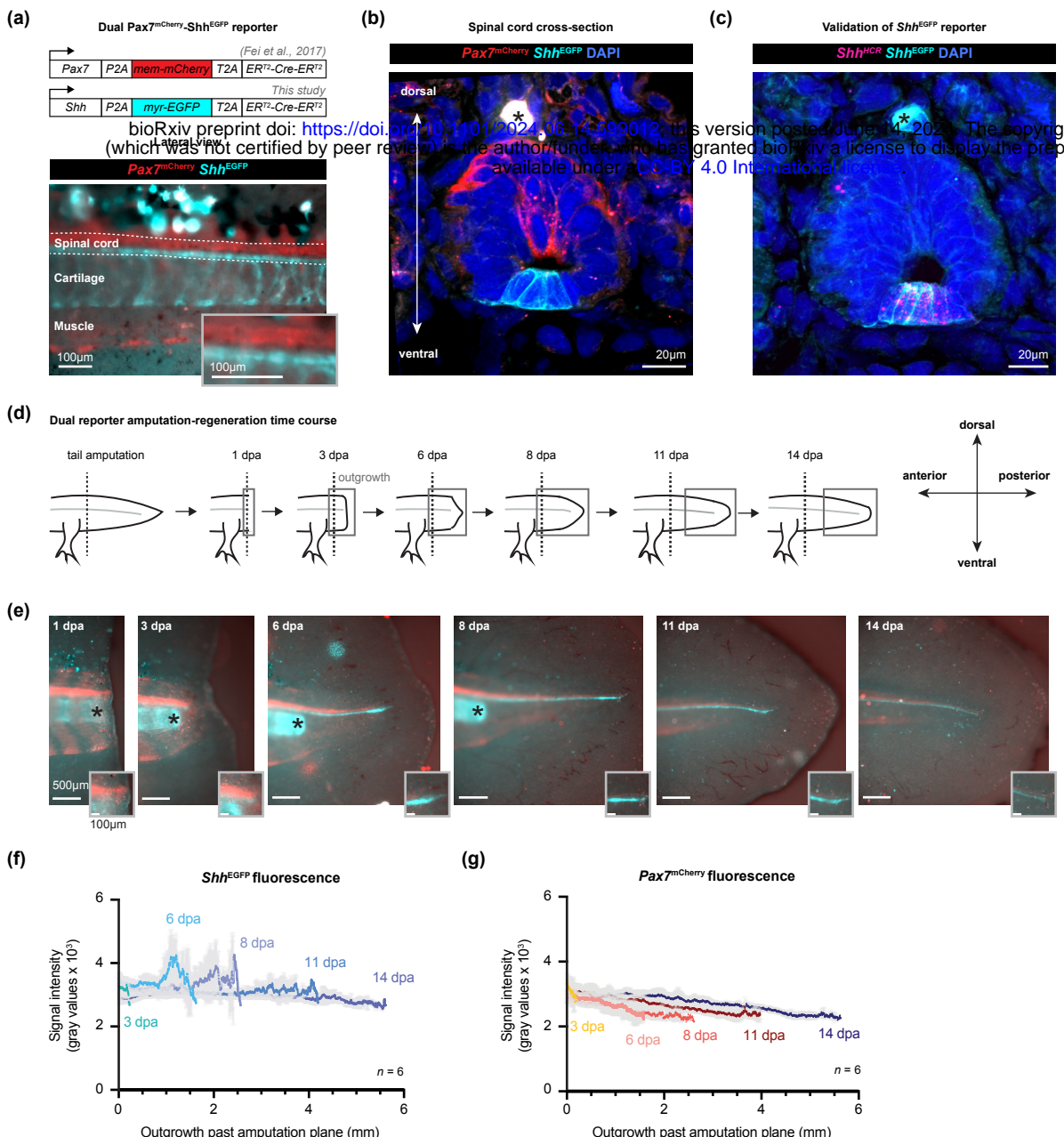


Figure 2. Live tracking of a dorsal-ventral reporter axolotl reveals a high Shh upregulation zone during regeneration.

(a) A dual transgenic axolotl to track dorsal-ventral gene expression in axolotl spinal cord. CRISPR/Cas9-mediated knock-in results in co-expression of mCherry and tamoxifen-inducible Cre from the Pax7 locus (Fei et al., 2017) or EGFP and tamoxifen-inducible Cre from the Shh locus (this study). Dual transgenics are heterozygous for each allele. A lateral view of a 2 cm axolotl reveals mCherry and EGFP expression on the dorsal and ventral sides of the spinal cord respectively. Additional expression is seen in muscle cell lineages (mCherry) and the cartilage rod (EGFP).

(b) Spinal cord cross section from a 5 cm dual transgenic axolotl at 14 dpa. Red and cyan depict endogenous Pax7^{mCherry-dERCre} and Shh^{EGFP-dERCre} fluorescence. DAPI labels nuclei. Asterisk indicates autofluorescence. Maximum intensity projection through 20 μm of tissue, acquired with confocal microscopy.

(c) Spinal cord cross section from a 5 cm dual transgenic axolotl at 14 dpa. Pax7^{mCherry-dERCre} is not depicted. Cyan depicts endogenous Shh^{EGFP-dERCre} fluorescence. Magenta is HCR labelling against endogenous Shh mRNA. 100% of Shh^{EGFP-dERCre}+ cells were Shh mRNA+ (n = 72 cells from 6 spinal cords). Asterisk indicates autofluorescence. Maximum intensity projection through 20 μm of tissue, acquired with confocal microscopy.

(d) An amputation-regeneration time course to measure changes in Pax7^{mCherry-dERCre} and Shh^{EGFP-dERCre} expression. Boxed areas represent images areas in (e).

(e) Widefield microscopy of regenerating tails from 3 cm axolotls. Insets are magnifications of the regenerating spinal cord tip. Asterisks indicate the amputated tip of the cartilage rod, which acts as an indicator of the amputation plane.

(f) Quantification of Shh^{EGFP-dERCre} fluorescent signal in the regenerating part of the spinal cord. Dark lines are mean intensity values averaged from n = 6 spinal cords per time point; pale lines indicate standard deviations.

(g) Quantification of Pax7^{mCherry-dERCre} fluorescent signal in the regenerating part of the spinal cord. Dark lines are mean intensity values averaged from n = 6 spinal cords per time point; pale lines indicate standard deviations.

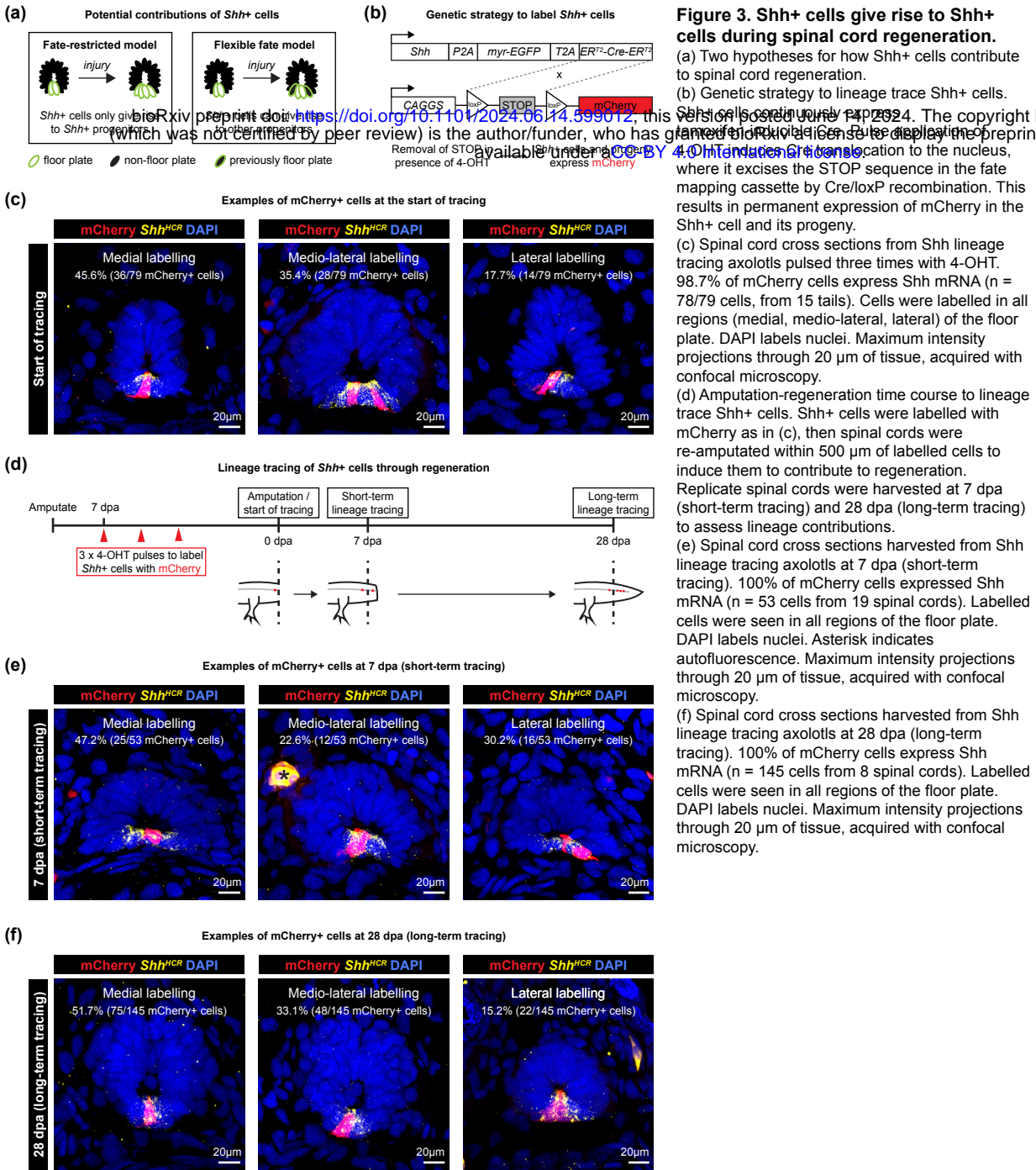


Figure 3. *Shh*⁺ cells give rise to *Shh*⁺ cells during spinal cord regeneration.

(a) Two hypotheses for how *Shh*⁺ cells contribute to spinal cord regeneration.

(b) Genetic strategy to lineage trace *Shh*⁺ cells.

Shh⁺ cells contribute to spinal cord regeneration. This version posted June 14, 2024. The copyright holder grants permission to display the preprint in perpetuity. It is made available under aCC-BY 4.0 International license.

(c) Spinal cord cross sections from *Shh* lineage tracing axolotls pulsed three times with 4-OHT. 98.7% of mCherry cells express *Shh* mRNA (n = 78/79 cells, from 15 tails). Cells were labelled in all regions (medial, medio-lateral, lateral) of the floor plate. DAPI labels nuclei. Maximum intensity projections through 20 μm of tissue, acquired with confocal microscopy.

(d) Amputation-regeneration time course to lineage trace *Shh*⁺ cells. *Shh*⁺ cells were labelled with mCherry as in (c), then spinal cords were re-amputated within 500 μm of labelled cells to induce them to contribute to regeneration. Replicate spinal cords were harvested at 7 dpa (short-term tracing) and 28 dpa (long-term tracing) to assess lineage contributions.

(e) Spinal cord cross sections harvested from *Shh* lineage tracing axolotls at 7 dpa (short-term tracing). 100% of mCherry cells expressed *Shh* mRNA (n = 53 cells from 19 spinal cords). Labelled cells were seen in all regions of the floor plate. DAPI labels nuclei. Asterisk indicates auto-fluorescence. Maximum intensity projections through 20 μm of tissue, acquired with confocal microscopy.

(f) Spinal cord cross sections harvested from *Shh* lineage tracing axolotls at 28 dpa (long-term tracing). 100% of mCherry cells express *Shh* mRNA (n = 145 cells from 8 spinal cords). Labelled cells were seen in all regions of the floor plate. DAPI labels nuclei. Maximum intensity projections through 20 μm of tissue, acquired with confocal microscopy.